sustainability

MDPI

Article

Integrated Performance Assessment of Polyurethane-Based Permeable Pavement Composites

Ernestas Ivanauskas [1,*], Šarūnas Čičinis [2], Algirdas Augonis [1], Gediminas Stelmokaitis [1] and Agnė Jucytė-Čičinė [3]

[1] Faculty of Civil Engineering and Architecture, Kaunas University of Technology, Studentu St. 48, LT-51367 Kaunas, Lithuania; algirdas.augonis@ktu.lt (A.A.); gediminas.stelmokaitis@ktu.lt (G.S.)
[2] Infrastructure Development Department, Klaipeda District Municipality Administration, Klaipedos St. 2, LT-96130 Gargzdai, Lithuania; sarunas.cicinis@klaipedos-r.lt
[3] Marine Research Institute, Klaipeda University, Universiteto Ave. 17, LT-92295 Klaipeda, Lithuania; agne.jucyte-cicine@ku.lt
* Correspondence: ernestas.ivanauskas@ktu.lt

Abstract

Permeable pavements are increasingly adopted to reduce urban runoff and support sustainable stormwater management; however, their long-term performance in cold regions is often limited by the need to maintain both hydraulic conductivity and durability under freeze–thaw cycles and de-icing salt exposure. This study investigates polyurethane (PU)-bound permeable composites based on granite aggregates for paver joint filling, permeable paver production, and monolithic permeable paving. This study provides a combined evaluation of aggregate gradation and PU binder content in relation to hydraulic performance, mechanical resistance, adhesion/cohesion, water absorption, and salt-freeze scaling resistance. Four mixtures were prepared using different combinations of 0/1 and 2/5 mm granite fractions and PU binder contents. The results showed that all mixtures exceeded the target permeability requirement of 2×10^{-5} m/s, while the coarse-only mixture with 3.0% PU binder provided the most balanced performance. This mixture achieved the highest permeability, the highest compressive and splitting tensile strength among the tested mixtures, the lowest water absorption, and the lowest surface scaling after 28 freeze–thaw cycles in 3% NaCl solution. The findings indicate that a coarse aggregate skeleton effectively bonded by the PU can support both rapid drainage and improved resistance to salt-freeze deterioration. However, further field validation under traffic loading, clogging, and long-term environmental exposure would be needed before full-scale application.

Keywords: permeable pavements; polyurethane binders; sustainable urban drainage; freeze–thaw resistance; permeable paver joints

Academic Editor: Piergiorgio Tataranni

Received: 2 May 2026
Revised: 20 May 2026
Accepted: 22 May 2026
Published: 1 June 2026

1. Introduction

Urban flooding and stormwater management have become major challenges in modern cities due to increasing rainfall intensity, climate change, and the continuous expansion of impermeable urban surfaces [1–3]. Conventional pavement systems, such as asphalt or dense concrete, prevent water infiltration into the soil and significantly increase surface runoff [4]. As a result, stormwater drainage systems are frequently overloaded, leading to flooding of streets, pedestrian areas, and parking areas [4,5].

Permeable pavement systems are increasingly developed as a solution supporting sustainable urban drainage systems (SUDS). They reduce surface runoff while contributing

to groundwater recharge, pollutant retention, and mitigation of the urban heat island effect [4,6–8]. Recent studies have increasingly focused on improving the long-term hydraulic and mechanical performance of permeable pavement materials under realistic environmental exposure conditions [9–12]. Several permeable pavement technologies have been developed, including porous asphalt, pervious concrete, and permeable interlocking concrete pavements [7,8,13]. Their performance depends on interconnected pore structures that allow water infiltration through the pavement layers [8,9].

Despite their environmental advantages, permeable pavements still face important limitations related to insufficient mechanical strength, clogging, and deterioration under freeze–thaw cycles and de-icing salt exposure [14–16]. Recent studies emphasize that the balance between permeability, structural integrity, pore connectivity, and durability remains one of the main challenges in the development of sustainable permeable pavement systems [10,12,17,18]. Highly porous materials often exhibit reduced resistance to mechanical loading and environmental degradation, particularly in cold-climate regions [15,16,19].

Polymer-based binders have recently gained attention as potential alternatives to traditional mineral or bituminous binders for permeable pavement applications [20]. Among them, polyurethane (PU) binders have demonstrated favourable adhesion to granular skeletons, elasticity, chemical stability, and resistance to environmental degradation while preserving pore connectivity in permeable pavement systems [21–24]. Furthermore, recent research has shown that the performance of PU-bound permeable systems is strongly influenced not only by binder type, but also by aggregate gradation, pore structure, and binder content [11,12,24,25]. Nevertheless, previous studies have mainly focused on hydraulic or mechanical performance separately, while comprehensive evaluation of permeability, mechanical strength, adhesion/cohesion, water absorption, and freeze–thaw durability under de-icing salt exposure remains limited, particularly for cold-climate applications.

Therefore, this study aimed to develop and evaluate PU-based permeable mixtures for joint filling, individual pavers, and monolithic paving with enhanced mechanical, hydraulic, and durability performance. Thus, the integrated assessment of aggregate gradation and PU binder content in relation to hydraulic conductivity, compressive and splitting tensile strength, adhesion/cohesion performance, water absorption, and salt-freeze durability was performed.

2. Materials and Methods

2.1. Materials

Granite aggregate fractions of 0/1 mm and 2/5 mm were used as the mineral skeleton of the PU-bound permeable composites. The 0/1 mm fraction was used to modify the fine aggregate content in mixtures M1-FC-3.0PU, M2-FC-2.5PU, and M3-FC-2.0PU, whereas the 2/5 mm fraction formed the coarse aggregate skeleton in all mixtures and was used as the only aggregate fraction in M4-C-3.0PU. The bulk density values, determined according to LST EN 1097-3:2002, were 1295 kg/m^3 for the 0/1 mm fraction and 1488 kg/m^3 for the 2/5 mm fraction.

The binder used in this study was a commercially available two-component PU-forming system obtained from an external commercial supplier for laboratory research purposes. The system was supplied as two separate liquid components: Component A, identified as the hardener, and Component B, identified as the resin. The components were mixed at a constant A:B mass ratio of 65:100 in all mixtures, according to the supplier's instructions. After mixing, the reactive system cured to form a PU binder phase, which bonded the granite aggregate particles at their contact points while preserving the open pore structure required for water permeability.

The A:B ratio of 65:100 was selected to provide sufficient aggregate bonding while maintaining a less brittle binder response suitable for permeable joint-filling and paving applications. The present study was designed as a performance-based evaluation of cured PU-bound granite aggregate composites rather than a chemical characterization of the individual liquid PU components. Therefore, the binder is described by its functional type, component ratio, curing conditions, and measured performance in the composite system.

To provide additional background on the selected PU binder system, supplementary binder-level stiffness data were obtained within the broader research programme. The flexural stiffness of the cured PU binder was found to depend on the hardener-to-resin ratio and temperature. For PU compositions 100/85, 100/75, and 100/65, the S(60) values determined according to LST EN 14771:2023 [26] were 73, 41, and 21 MPa at 20 °C and 218, 204, and 138 MPa at −8 °C, respectively. These data indicate that the mechanical response of the cured PU phase is temperature-dependent and support the importance of binder ratio selection for PU-bound permeable systems.

Additional binder drainage tests were also performed according to LST EN 12697-18:2017 [27] using the perforated basket method. No measurable binder drainage was observed for any of the investigated mixtures after 3 h at 5, 10, 15, 20, 25, or 50 °C, confirming the practical stability of the mixtures within the investigated handling temperature range. No additional admixtures, pigments, fillers, or chemical modifiers were added to the mixtures.

2.2. Mixture Design and Specimen Preparation

Unless otherwise stated, three replicate specimens (n = 3) were prepared and tested for each mixture and each test method; reported values represent the mean value with the corresponding standard deviation (SD). During the experiments, the production process for the PU mortar was identical across all mixture compositions. After weighing out the required amounts of components, the two-component PU was mixed first. For this purpose, the PU hardener (Component A) and resin (Component B) were poured into a 15 L plastic container and mixed for 30 s at low speed using an electric mortar mixer equipped with a paddle mixer until a homogeneous mass was achieved. The exact rotational speed was not recorded because the mixer was operated using a predefined low-speed setting. Afterward, the appropriate amounts of air-dried granite fractions 0/1 and 2/5 were added to the same container. The entire mixture was then vigorously mixed at high speed for 2 min using the same electric mixer. The resulting homogeneous mixture was placed into grease-coated molds using a forming spatula. The formed specimens were cured for 24 h in molds and then stored under laboratory conditions at 20 ± 2 °C and 55 ± 10% relative humidity until testing at 28 days.

The bulk densities of the granite aggregates used in the tests are presented in Table 1. To produce a suitable jointing compound for filling the joints between the pavers, with sufficient water permeability and meeting other target properties, four different compositions were designed. The first three compositions were produced using a mixture of 0/1 and 2/5 granite aggregate and a PU binder of 3%, 2.5%, and 2%. The fourth composition contained coarse granite aggregate fr. 2/5 only. To improve readability, descriptive mixture labels were introduced: M1-FC-3.0PU (Mixture I), M2-FC-2.5PU (Mixture II), M3-FC-2.0PU (Mixture III), and M4-C-3.0PU (Mixture IV), where FC denotes fine-plus-coarse aggregate gradation and C denotes coarse-only aggregate gradation. The compositions of all water-permeable mixtures used for forming joints between pavers and for forming the pavers themselves are presented in Table 2.

Table 1. Bulk density of granite aggregate, size 0/1 and 2/5. Average values are presented as mean ± SD.

Parameter, Unit of Measurement, Test Method Code	Fraction	Average
Bulk density, kg/m^3 (LST EN 1097-3:2002) [28]	0/1	1295 ± 4
	2/5	1488 ± 2

Table 2. Compositions of water–permeable PU mixtures designed for joints between pavers and for pavers themselves, in kilograms per cubic meter (kg/m^3). Descriptive labels indicate aggregate gradation and PU binder content.

Components	Mixtures			
	M1-FC-3.0PU (I)	M2-FC-2.5PU (II)	M3-FC-2.0PU (III)	M4-C-3.0PU (IV)
Total amount of PU binder (A + B)	44.1	36.8	29.4	44.3
Granite aggregate fr. 0/1	735	735	735	–
Granite aggregate fr. 2/5	735	735	735	1475
Percentage of PU binder by weight of fillers, %	3	2.5	2	3
Component A *	17.4	14.5	11.6	17.4
Component B *	26.7	22.3	17.8	26.8

Note: * The PU binder was produced by maintaining a ratio of hardener A to resin B of 65:100.

2.3. Air Void Content Testing

The air void content (T, %) of the PU–bound mixtures was determined from the maximum density and the bulk density of the specimens. The maximum density ρ_{mh} (mg/m^3) was determined in accordance with LST EN 12697–5:2019 [29] using a hydrostatic (pycnometer) approach. Prior to weighing, entrapped air was removed by mechanical agitation and ultrasonic conditioning in a water bath for 30 min at 22 ± 1 °C to ensure stable readings. Water density was corrected according to the bath temperature, and ρ_{mh} was calculated using the hydrostatic principle.

The bulk density ρ_p (mg/m^3) of the cured specimens was determined by hydrostatic weighing (Archimedes' method), based on the mass of the dry specimen in air and its apparent mass in water. For each mixture, replicate measurements were used to calculate the mean with the corresponding standard deviation value.

2.4. Determination of Compressive and Flexural Strength

Compressive strength tests of the PU mortar (mastic), intended for filling joints between paving stones, were performed in accordance with the LST EN 1015–11:2020 standard [30]. The prepared PU mortar was poured into two 40 × 40 × 160 mm molds. After 24 h, the hardened specimens were removed from the molds and left for 27 days in a climatic chamber at a temperature of 20 ± 2 °C and a water vapor transmission rate of 45 ± 15 g/(m^2·h). After 28 days of curing, the flexural and compressive strengths were determined. The flexural strength was determined using a "Toni Technik" press with appropriate piston tips (Figure 1).

Figure 1. Determination of the flexural strength.

The compressive strength of the specimens was determined by placing the separated halves of the specimen between two support plates made of steel with a hardness of at least 600 HV (measured according to the Vickers hardness scale), with the following dimensions: width 40.0 mm ± 0.1 mm, length 40.0 mm ± 0.1 mm, and thickness 10.0 mm ± 0.1 mm.

2.5. Resistance to the Freeze–Thaw Cycles

Freeze–thaw resistance tests of the mortar (mastic) intended for filling joints between paving blocks under de-icing salt exposure were conducted in accordance with the CF/CDF test method, as referenced in Paragraph 197 of Chapter IX of the methodological guideline MN TRINKELĖS 14 [31] and described in CEN/TS 12390-9:2016 [32]. A 3% NaCl aqueous solution was used as the de-icing salt medium. The specimens were prepared, measuring 40 × 40 × 160 mm in accordance with the requirements of LST EN 1015–11:2020 standard [30]. After 24 h, the hardened PU mortar specimens were removed from the molds and left for 27 days in a climatic chamber, where the temperature was maintained at 20 ± 2 °C and the water vapor transmission rate at 45 ± 15 g/(m^2·h). After 28 days, the specimens were dried at 110 ± 10 °C for 24 h in a ventilated convection oven until a constant mass (M1) was achieved. After cooling to a temperature of 20 ± 2 °C, the samples were weighed to an accuracy of 0.1 g and placed in a temperature-controlled chamber. In the chamber, the specimens were immersed at 5 ± 0.1 mm into a 3% aqueous NaCl solution. Since the specimen rested on 5 mm high supports, the total height of the cooling fluid layer in the cells during the test was 10 ± 1 mm. The specimens were cooled and thawed according to the temperature and time curve (Figure 2). After 4 ± 1; 6 ± 1; 14 ± 1, and 28 stages of the freeze–thaw cycle, with the chamber temperature above 15 °C, the specimens were removed from the chamber, and the debris that has fallen off the samples was collected from the bottom, washed with the tap water, and dried in a ventilated convection dryer for 24 h at a temperature of 110 ± 10 °C. The residues were cooled for 60 ± 5 min at 20 ± 2 °C and 65 ± 5% relative humidity and then weighed to the nearest 0.1 g. The remaining specimens were returned to the cells for subsequent freeze–thaw cycles. The 3% NaCl test solution was replaced with a fresh solution after each measurement interval.

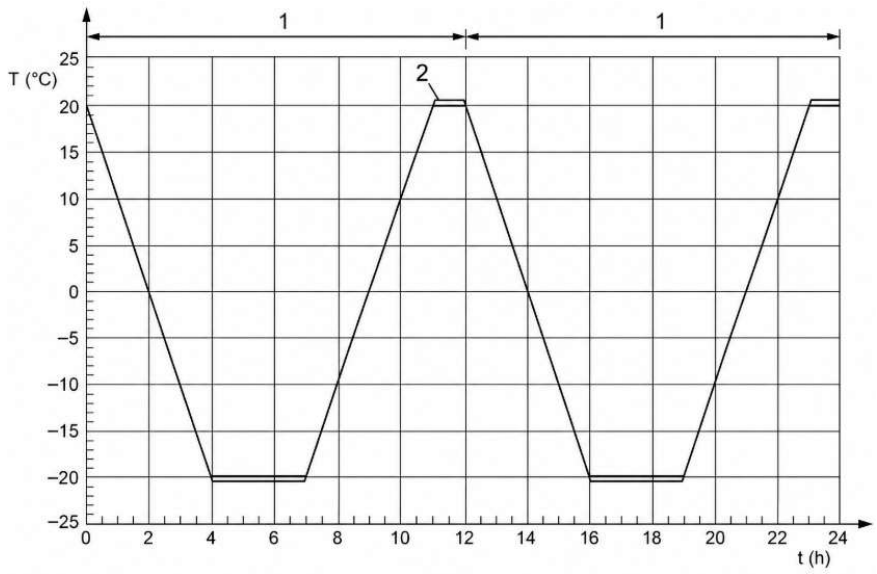

Figure 2. Temperature curve in the chamber. Legend: 1—12 h freeze–thaw cycle; 2—permissible temperature deviations from the set value.

2.6. Determination of the Adhesion Strength

Tests of the adhesion strength of the PU mortar intended for filling joints between paving stones were conducted in accordance with the requirements of LST EN 1015–12:2016 standard [33].

Tensile adhesion strength was evaluated by applying a layer of PU mortar, intended for filling joints between paving stones, onto different substrates, including concrete and PU surfaces representative of paving elements. In addition, the cohesive strength of the mortar mixtures was assessed. Based on common pavement practice, the target tensile adhesion strength for the investigated application was $\geq$1.5 MPa. Testing was carried out using a concrete slab as the base substrate. The surface was coated with a layer of the mortar mixture with a thickness ranging from 10 to 60 mm. During testing, the tensile strength was required to exceed the expected adhesion strength of the applied material. After curing for 28 days, test specimens were prepared by drilling annular grooves with a diameter of 50 mm and a depth of approximately 10 mm. The test area was cleaned thoroughly prior to bonding. Circular steel discs (50 $\pm$ 0.5 mm in diameter and 25 mm in thickness) were bonded to the surface using "Bison Epoxy 5 Minutes" adhesive. Adhesion strength was measured using a "DYNA Z16" device (Proceq, Schwerzenbach, Switzerland) (maximum load 16 kN, accuracy 0.01 MPa). During testing, the tensile loading rate was selected according to Table 2 of LST EN 1015–12:2016 [33], considering the expected strength.

2.7. Determination of the Splitting Tensile Strength

Splitting tensile strength tests were conducted on PU-bound paving blocks (pavers) manufactured from mixtures I–IV in accordance with the methodological guidelines and conformity testing of LST EN 1338:2003—Annex F [34]. Paving stones for testing were made of a PU mixture (compositions I–IV) and manufactured at 200 $\times$ 100 $\times$ 60 mm dimensions. The test procedure involved soaking specimens in water at a temperature of 20 $\pm$ 5 °C for 24 $\pm$ 3 h before testing. The soaked specimen block was placed in the testing apparatus with load distribution bars on the upper and lower surfaces to contact the supports. It was verified that the axes of the load distributing strips and the supports were in line with the splitting plane of the paving stone. The apparatus consisted of two rigid supports with a contact surface radius of 75 $\pm$ 5 mm. The two rigid supports were set to be in the same vertical plane with a tolerance of $\pm$1 mm at the edges. The upper support was mounted

so that it could rotate about its transverse axis. This apparatus, together with the concrete block, was placed between the plates of a hydraulic press (Figure 3).

Figure 3. The testing process of a physical sample in the device.

The two load distribution strips were set to be 15 ± 1 mm wide (b), (4 ± 1) mm thick (a), and at least 10 mm longer than the expected failure plane. During the test, the load was increased at a constant rate corresponding to a stress increase of 0.05 ± 0.01 MPa/s. According to the requirements of LST EN 1338:2003 [34], when the test sample consists of eight pavers or fewer, the splitting tensile strength (T) of each paver shall be not less than 3.6 MPa.

2.8. Water Absorption

The water absorption of pavers produced using mixtures I–IV (Table 2) was determined in accordance with Annex E of LST EN 1338:2003 [34]. The pavers were placed on a grid and immersed in water at a temperature of 20 ± 5 °C, ensuring a minimum spacing of 15 cm between specimens. The water level was maintained at least 2 cm above the surface of the pavers. At 24 h intervals, the specimens were removed, surface–dried, and weighed to determine the saturated mass M1 (g). The final value of M1 was recorded when the difference between two consecutive measurements was less than 0.1%. Subsequently, the specimens were dried in a forced–circulation oven at 105 ± 5 °C, maintaining a minimum spacing of 15 cm between them. The dry mass M2 (g) was determined at 24 h intervals. The final value of M2 was recorded when the difference between two consecutive measurements was less than 0.1%.

2.9. Water Permeability Test

Water permeability was determined in accordance with LST EN 12697–19:2020 standard [35]. Two testing configurations were used to evaluate flow through the specimens: vertical flow (standard method) and horizontal flow. For each mixture, three specimens were tested. The permeability coefficient was determined separately for each flow direction, and the reported value represents the average of the test results obtained from all specimens. The specimens were formed as cylindrical rings with a diameter of 101.1 mm and a height of 42.1 mm. Three specimens were prepared for each mixture type under the same conditions as those used for compressive strength testing.

3. Results and Discussion

3.1. Air Void Content Testing

The air void content and density related parameters of the PU-bound mixtures are summarized in Table 3, providing the basis for interpreting permeability and durability performance. The results show a clear trend of increasing maximum density from Mixture I to Mixture IV. The highest average maximum density was observed in Mixture IV (2.607 ± 0.032 mg/m^3), while the lowest was in Mixture II (2.426 ± 0.090 mg/m^3). Mixtures III and IV exhibited higher densities compared to Mixtures I and II, indicating improved packing characteristics of the aggregate structure.

Table 3. Average maximum density, bulk density, and air void content of mixtures. Values are presented as mean ± SD.

Mixture	Maximum Density ρ_{mh}, mg/m^3	Bulk Density ρ_p, mg/m^3	Air Void Content T, %
I	2.436 ± 0.043	1.511 ± 0.058	37.94 ± 3.20
II	2.426 ± 0.090	1.516 ± 0.017	37.40 ± 2.93
III	2.525 ± 0.028	1.538 ± 0.042	39.06 ± 1.71
IV	2.607 ± 0.032	1.528 ± 0.015	41.04 ± 1.19

However, despite the higher density, Mixture IV also showed the highest air void content (41.04% ± 1.19), demonstrating that increased density does not directly correspond to lower void content. The simultaneous occurrence of the highest maximum density and highest air void content in Mixture IV can be explained by distinguishing between solid-phase density and compacted skeleton structure. Maximum density represents the theoretical density of the mixture without air voids and is influenced by the mineral density of the aggregate and binder content. In contrast, air void content is calculated from the difference between maximum density and bulk density and is strongly affected by aggregate packing characteristics. The coarse-only 2/5 mm fraction used in Mixture IV likely formed an open aggregate skeleton with larger interparticle voids, while the solid constituents themselves had a relatively high maximum density. Therefore, high maximum density and high air void content can coexist in this type of permeable composite. Since direct pore-structure imaging was not performed, pore connectivity in the present study is discussed only as an indirect interpretation based on the combined air void, permeability, and water absorption results. This approach is consistent with previous studies showing that aggregate gradation, void content, permeability, and water absorption are closely related to the pore structure and hydraulic behavior of pervious materials [9,10,36,37].

3.2. Determination of the Compressive and Flexural Strength

After conducting flexural and compressive strength tests on specimens prepared from mixtures I–IV of PU mortar intended for joint filling, it was found that Mixture IV exceeded the target compressive strength of 5 MPa, which was used in this experimental programme as an application-specific performance target for PU mortar intended for paver joint filling rather than as a universal standard requirement for all permeable pavement materials (Figure 4).

Based on these results, Mixture IV would be recommended for filling the joints between pavers. Despite the intentionally high porosity, Mixture IV achieved the target compressive strength (≥5 MPa) and exhibited the best overall mechanical performance among the investigated formulations. This indicates that the coarse aggregate skeleton, combined with 3% PU binder, formed an efficient load–transfer framework, in which binder bridges between coarse particles contribute to the stiffness and resistance to crack

initiation [25]. Since direct pore-structure imaging was not performed, the interpretation of pore connectivity was based on air void content, water permeability, water absorption, and mechanical performance results. Similar studies on pervious materials have shown that aggregate structure and drainage-path connectivity can strongly influence mechanical and hydraulic properties [9,36].

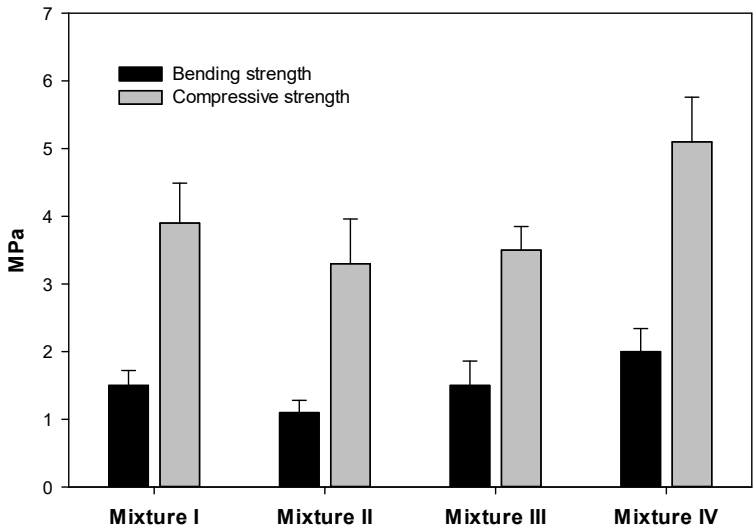

Figure 4. Results of bending and compressive strength tests on specimens. Data is presented as mean (n = 6) ± SD, indicated as error bars.

3.3. Resistance to the Freeze–Thaw Cycles

After testing the freeze–thaw resistance of specimens prepared from PU mortar mixtures I–IV intended for joint filling in a 3% NaCl solution (de-icing salt exposure), Mixture III, with the lowest binder content (2%), exhibited the poorest performance. The average mass loss after 28 cycles was the highest (S28 = 0.513 kg/m^2). In contrast, Mixture IV showed the best performance, with an average mass loss value (S28 = 0.109 kg/m^2). Meanwhile, Mixtures I and II exhibited mass losses approximately 2.5 times higher than those of Mixture IV (Table 4).

Table 4. The mass of loose material from 1 m^2 of the pavement surface after 28 freeze–thaw cycles (S_{28}). Values are presented as mean ± SD, and determined to the nearest 0.1 g.

Mixture	$m_{s,n}$, g	$m_{s,before}$, g	$(m_{s+f} - m_f)$, g	S_{28}, kg/m^2
I	1.60 ± 0.92	0.80 ± 0.46	0.80 ± 0.46	0.248 ± 0.145
II	1.60 ± 0.95	0.80 ± 0.40	0.80 ± 0.56	0.247 ± 0.147
III	3.30 ± 1.91	1.63 ± 1.01	1.67 ± 0.90	0.513 ± 0.300
IV	0.70 ± 0.00	0.30 ± 0.00	0.40 ± 0.00	0.109 ± 0.000

Notes: $m_{s,n}$—mass of scaled material from the specimen after n freeze–thaw cycles. $m_{s,before}$—mass of scaled material from the specimen recorded during the previous inspection. m_{s+f}—mass of the scaled material together with the filter after n freeze–thaw cycles. m_f—mass of the filter. S_{28}—mass of scaled material from 1 m^2 of pavement surface after 28 freeze–thaw cycles, kg/m^2.

The results indicate that Mixture IV was the most suitable formulation for joint filling under freeze–thaw conditions with de-icing salt exposure. Its mass loss per unit surface area was approximately two times lower than that of Mixtures I and II and almost five times lower than that of Mixture III. These differences are important for cold-climate applications, where repeated freezing, thawing, and salt exposure can accelerate surface scaling and particle loss.

The inferior performance of Mixture III is most likely related to its lower PU binder content (2%), which may have reduced cohesion between aggregate particles and increased

susceptibility to salt-frost damage, as reported for porous and cementitious materials exposed to scaling conditions [38]. In contrast, the superior performance of Mixture IV can be attributed to the combined effect of higher cohesive strength, lower water absorption, and high permeability. Higher cohesion may reduce raveling under ice crystallization pressure, lower water absorption limits the uptake of water-salt solution, and high permeability may support more effective drainage during freeze–thaw cycling [39–41]. From a life-cycle perspective, reduced scaling implies longer service life and lower maintenance requirements, supporting the use of PU-bound coarse-aggregate systems in sustainable pavement applications exposed to cold climates and de-icing salts [42,43].

3.4. Cohesive and Adhesive Strength Determination

The weakest internal cohesion was obtained for mixtures I and III, with the average values of 0.47 and 0.72 MPa, respectively. The highest cohesive strength was obtained for mixtures II and IV, with the average values of cohesive strength of 1.00 and 1.59 MPa, respectively. The distribution of the measured values is presented in Figure 5.

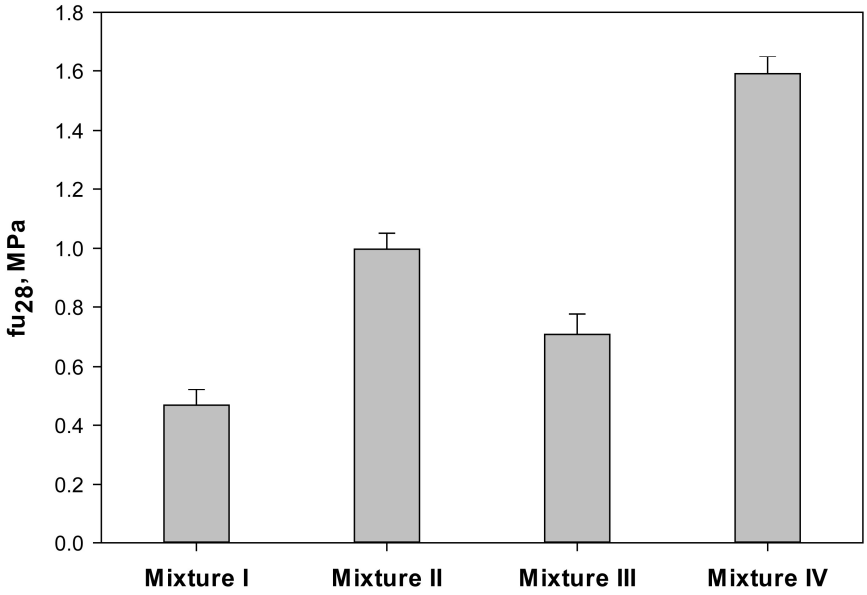

Figure 5. Cohesive bond strength of different PU mixtures (I–IV). Data is presented as mean (n = 15) ± SD, indicated as error bars.

As shown in Figure 5, Mixture IV exhibited the highest internal cohesive strength and would, therefore, be recommended for filling joints between concrete or PU paving elements.

Based on the test standard, failure modes can be classified according to the fracture location: (i) cohesive failure within the PU-bound layer, (ii) failure within the adhesive layer, and (iii) failure within the substrate.

The average adhesion strength to the concrete substrate was 0.38, 0.82, 0.58, and 1.24 MPa for Mixtures I–IV, respectively, while slightly lower values were obtained for the PU substrate: 0.31, 0.71, 0.51, and 1.08 MPa, respectively. A consistent trend was observed for both substrates, with Mixture IV showing the highest adhesion and Mixture I the lowest, resulting in the overall ranking: IV > II > III > I. Adhesion to concrete was consistently higher than to PU, which can be attributed to the rougher and more porous surface of concrete, promoting mechanical interlocking [22,25]. In contrast, PU substrates are smoother and less absorbent, resulting in reduced mechanical bonding. For all mixtures, adhesion strength was lower than the corresponding cohesive strength, indicating that failure is more likely to initiate at the interface rather than within the bulk material. This

highlights the importance of the interfacial zone for durability under thermal, moisture, and mechanical loading.

Accordingly, the adhesion of the investigated PU-bound mixtures, intended for filling joints between paving elements with different surface types, was evaluated on a concrete substrate and, separately, on a PU substrate representative of PU paving stones/tiles or continuous PU pavement. The average adhesion strength values (MPa) obtained from the tests are presented in Figure 6.

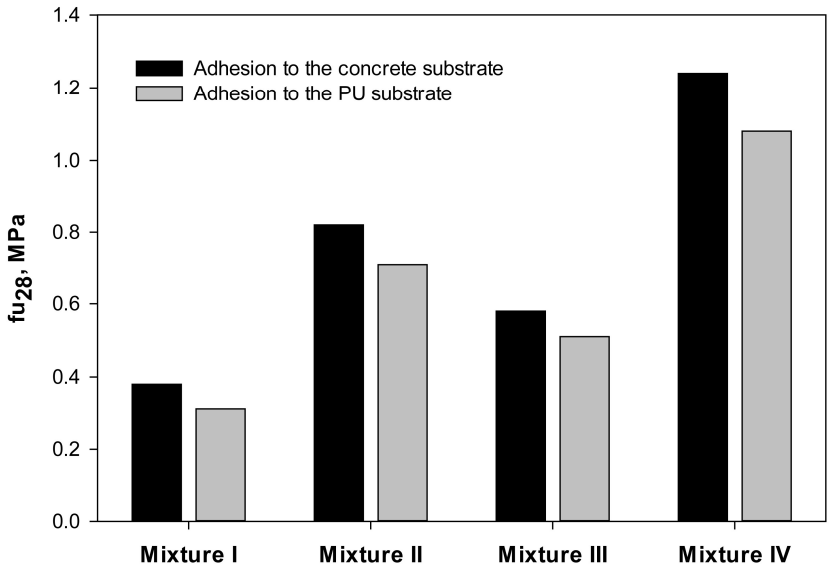

Figure 6. Adhesion strength of different pavement mixtures (I–IV) to concrete and PU substrates.

Adhesion results indicate that interface performance may govern the long–term functionality of PU jointing and overlays. Mixture IV achieved the highest cohesive strength (1.59 MPa) (Figure 5) and the highest adhesion to both concrete (1.24 MPa) and PU substrates (1.08 MPa). Adhesion was consistently higher to concrete than to PU, which can be explained by the rougher and more porous concrete surface, enabling mechanical interlocking. Importantly, adhesion values remained below the cohesive strength (Figure 5), implying that failure is more likely to initiate at the interface zone rather than within the bulk mixture. For practical applications, this suggests that surface preparation and substrate texture will be critical, particularly for monolithic PU paving or PU to PU bonding, where the interface is smoother and less absorbent.

3.5. Determination of Splitting Tensile Strength

The results of the tensile strength at break tests conducted on different mixture compositions (I–IV) are presented in Table 5.

The results show that Mixture IV exhibited the highest splitting tensile strength (1.22 ± 0.01 MPa), while Mixture III showed the lowest value (0.85 ± 0.01 MPa). The superior performance of Mixture IV can be attributed to the use of coarse granite aggregate (fraction 2/5) combined with sufficient binder content, which promotes the formation of a stable load–bearing skeleton. Splitting tensile strength followed the same performance ranking observed for compressive strength and durability indicators. This supports the interpretation that adequate binder content and a stable coarse aggregate structure enhance crack resistance in porous composites, as also reported in studies on pervious materials [18].

Table 5. Results of the tensile strength at the break test. Values are presented as mean ± SD; the correction factor for all mixtures (I–IV) was k = 0.87.

Mixture	Fracture Length l, mm	Thickness of the Fracture Plane t, mm	Fracture Area S, mm^2	Fracture Load P, kN	Fracture Load per Unit Length F, N/mm	Splitting Tensile Strength T_{vid}, MPa
I	194.8 ± 0.0	57.3 ± 0.1	11,150.26 ± 6.82	20.3 ± 0.2	104.0 ± 1.0	1.01 ± 0.01
II	194.5 ± 0.0	56.5 ± 0.0	10,985.21 ± 2.11	21.6 ± 0.1	111.3 ± 0.6	1.09 ± 0.01
III	194.6 ± 0.1	50.6 ± 0.1	9853.25 ± 18.33	15.2 ± 0.2	78.0 ± 1.0	0.85 ± 0.01
IV	195.6 ± 0.1	57.0 ± 0.0	11,144.85 ± 1.93	24.6 ± 0.2	126.0 ± 1.0	1.22 ± 0.01

For permeable pavers and monolithic applications, higher splitting tensile strength is particularly important, as it is associated with improved resistance to cracking under localized loads, thermal stresses, and freeze–thaw-induced microcracking.

3.6. Water Absorption

The results of water absorption tests on finished pavers made with I–IV are presented in Table 6. In all cases, the average water absorption values were notably lower than the target limit of 6% by mass and can be classified as Class B according to LST EN 1338:2003 [34].

Table 6. Water absorption of pavers made with mixtures I–IV. Values are presented as mean ± SD.

Mixture	Mass of the Wet Sample M_1, g	Dry Weight M_2, g	Water Absorption W_a
I	2178.0 ± 8.4	2169.0 ± 4.2	0.41 ± 0.19
II	2176.6 ± 8.6	2167.5 ± 3.7	0.42 ± 0.23
III	2189.5 ± 1.6	2170.8 ± 7.5	0.86 ± 0.39
IV	2195.3 ± 4.4	2191.3 ± 4.8	0.18 ± 0.03

Values for all mixtures ranged from 0.18 to 0.86%, far below typical limits for concrete paving units. Mixture IV exhibited the lowest water absorption, which is consistent with the improved resistance to salt and frost-induced scaling observed in CF/CDF testing. The low absorption suggests that the PU binder effectively limits capillary suction within the composite, even when the overall void content is high. This highlights an important distinction for permeable systems: high interconnected macroporosity can support infiltration, while low capillary porosity and reduced sorptivity can improve durability in freeze–thaw environments, as reported in other studies on pervious materials [12,17,44].

3.7. Water Permeability Test

The water permeability results measured in vertical and horizontal directions are presented in Tables 7 and 8, respectively, to assess infiltration capacity and directional flow behavior. The test results show that all samples tested meet the requirements specified in the assignment and are substantially more permeable to water (water permeability must be $\geq 2 \times 10^{-5}$ m/s). Therefore, PU products made from all four types of studied mixtures could be used for both filling joints between pavers, the production of pavers, and the installation of continuous paving, from the perspective of water permeability.

The highest water permeability was recorded for Mixture IV, with Kv = 4.37 ± 0.21 × 10^{-3} m/s and Kh = 3.87 ± 0.04 × 10^{-3} m/s. The lowest water permeability was determined for Mixture III, with Kv = 2.27 ± 0.06 × 10^{-3} m/s and Kh = 1.87 ± 0.07 × 10^{-3} m/s. The test data indicate that vertical water permeability is slightly higher than horizontal permeability, which may reflect directional differences in the open flow paths formed during specimen preparation, as commonly observed in permeable materials [45–49].

However, since direct pore-structure imaging was not performed, this interpretation should be treated as indirect and based on the measured hydraulic response. These findings are relevant for further development related not only to the use of PU mortar for filling joints between pavers but also to the use of PU for the production of pavers or the installation of a monolithic pavement. To improve the physical and mechanical properties of the products, the latter can be formed with a higher density. To achieve this goal, it is advisable to model both the composition of the PU mortar and the amount of binder, as well as to apply a compression/pressing forming method as suggested in recent studies on the optimization of pervious materials [50,51].

Table 7. Results of the water permeability test conducted in the vertical direction. Permeability rate and coefficient values are presented as mean ± SD.

Mixture	Ambient Temperature T, °C	Filtration Time, t, s	Water Permeability Rate Q, m^3/s	Water Permeability Coefficient Kv, m/s
I	21.5	40.0	$(2.07 \pm 0.04) \times 10^{-4}$	$(3.60 \pm 0.10) \times 10^{-3}$
II	22.0	35.0	$(2.40 \pm 0.00) \times 10^{-4}$	$(4.10 \pm 0.00) \times 10^{-3}$
III	21.0	60.0	$(1.30 \pm 0.02) \times 10^{-4}$	$(2.27 \pm 0.06) \times 10^{-3}$
IV	22.0	35.0	$(2.49 \pm 0.12) \times 10^{-4}$	$(4.37 \pm 0.21) \times 10^{-3}$

Table 8. Results of the water permeability test conducted in the horizontal direction. Permeability rate and coefficient values are presented as mean ± SD.

Mixture	Ambient Temperature T, °C	Filtration Time, t, s	Water Permeability Rate Q, m^3/s	Water Permeability Coefficient Kh, m/s
I	21.0	30.0	$(3.22 \pm 0.03) \times 10^{-4}$	$(3.16 \pm 0.03) \times 10^{-3}$
II	21.5	30.0	$(3.51 \pm 0.07) \times 10^{-4}$	$(3.45 \pm 0.07) \times 10^{-3}$
III	20.0	40.0	$(1.90 \pm 0.07) \times 10^{-4}$	$(1.87 \pm 0.07) \times 10^{-3}$
IV	22.0	20.0	$(3.94 \pm 0.04) \times 10^{-4}$	$(3.87 \pm 0.04) \times 10^{-3}$

All mixtures exceeded the required permeability threshold ($\geq 2 \times 10^{-5}$ m/s), confirming suitability for stormwater infiltration applications. Mixture IV showed the highest permeability, whereas Mixture III had the lowest. Vertical permeability was slightly higher than horizontal, which may reflect directional differences in pore alignment during specimen preparation. When combined with the durability outcomes, Mixture IV offers the most favorable multi–criteria profile: high infiltration capacity together with low scaling and low water absorption, which is essential for sustainable pavements exposed to increasingly variable precipitation patterns and de-icing salt applications. Compared with traditional permeable pavement systems such as porous asphalt and pervious concrete, the investigated PU-bound composites provide very high hydraulic conductivity and low water absorption [8,10,23,46,51]. However, their compressive strength remains relatively low compared with conventional structural pavement materials, which may limit their application under heavy traffic loading [18,44,51]. Therefore, the main advantage of the proposed mixtures is not high load-bearing capacity for heavy traffic, but the combination of permeability, low capillary water uptake, salt-freeze resistance, adhesion, and binder stability for joint filling and light-traffic permeable pavement applications.

3.8. Durability-Related Performance and Practical Implications

The improved durability-related performance of Mixture IV can be attributed to the combined effects of several measured properties. First, the coarse aggregate skeleton

provided high permeability, allowing water and a salt solution to drain through the composite rather than remain trapped within capillary pores, consistent with previous findings that pore connectivity and permeability strongly affect the durability of pervious materials [9,10,17]. Second, the 3.0% PU binder content provided sufficient cohesion between aggregate particles, reducing particle loss during freeze–thaw cycling. Third, the very low water absorption indicates limited capillary uptake, reducing the amount of freezable water retained in the composite, which is important for resistance to frost and salt scaling [17,38,44]. Fourth, the relatively high adhesion values to concrete and PU substrates suggest improved interfacial integrity, which is important for joint filling and overlay applications. Finally, additional binder drainage tests indicated no measurable binder drainage at 5–50 °C, supporting the practical stability of the mixtures during handling and placement. Therefore, the durability improvement should be interpreted as a combined effect of drainage capacity, low water retention, higher cohesive strength of the PU-bound aggregate skeleton, and binder stability rather than as a result of porosity alone.

3.9. Limitations and Future Work

Several limitations should be noted. First, the compressive strength values obtained in this study are lower than those typically required for conventional heavily trafficked concrete or asphalt pavement layers. Therefore, the investigated PU-bound permeable composites should be considered primarily for joint filling, pedestrian areas, bicycle paths, light-traffic permeable surfaces, parking areas, landscape pavements, or monolithic permeable layers where hydraulic performance and salt-freeze durability are critical. Second, fatigue performance under cyclic traffic loading was not evaluated and should be addressed in future research. Third, this study was designed as a performance-based evaluation of cured PU-bound granite aggregate composites; therefore, detailed chemical characterization of the commercial PU binder and direct pore-structure imaging were outside the scope of the present work. Future studies could include FTIR, SEM, XRD, or optical microscopy to better relate binder chemistry and pore structure to long-term performance. Finally, long-term field validation under real traffic, clogging, maintenance, and environmental exposure conditions is required before full-scale application.

4. Conclusions

The study demonstrated that PU-bound granite aggregate mixtures can be tailored for permeable pavement applications where hydraulic capacity and durability under de-icing salt exposure must be balanced. The integrated evaluation showed that aggregate gradation and PU binder content strongly affected permeability, water absorption, mechanical performance, adhesion/cohesion, and salt-freeze scaling resistance.

Among the investigated mixtures, M4-C-3.0PU (coarse 2/5 mm aggregate with 3.0% PU binder) provided the most favorable multi-criteria performance. It achieved the highest hydraulic conductivity, the highest compressive and splitting tensile strength among the tested mixtures, the lowest water absorption, and the lowest surface scaling after 28 CF/CDF cycles in 3% NaCl solution.

The results indicate that improved durability was not governed by total porosity alone. Instead, it was associated with the combined effect of an open drainage skeleton, limited capillary water uptake, higher cohesive strength of the PU-bound mixture, and improved adhesion to concrete and PU substrates. Additional binder-level and binder-drainage information supports the interpretation that PU ratio and binder stability are important for the practical performance of these composites.

The proposed mixtures should not be considered direct substitutes for conventional heavy-traffic structural pavement materials. Their most suitable potential applications

include joint filling, pedestrian and bicycle areas, parking areas, light-traffic permeable surfaces, and monolithic permeable layers in cold-climate regions. Furthermore, future work should ideally include fatigue testing, field validation, clogging and maintenance assessment, as well as direct chemical, mineralogical, and/or microstructural characterization.

Author Contributions: Methodology, E.I., Š.Č., A.A. and G.S.; Validation, A.J.-Č.; Formal analysis, E.I., A.A., G.S. and A.J.-Č.; Investigation, E.I., A.A. and G.S.; Resources, A.J.-Č.; Data curation, E.I., Š.Č. and A.J.-Č.; Writing—original draft, E.I., A.A. and A.J.-Č.; Writing—review and editing, E.I. and Š.Č.; Visualization, A.J.-Č.; Supervision, Š.Č.; Project administration, A.J.-Č. All authors have read and agreed to the published version of the manuscript.

Funding: The research was conducted under contract No. 04-02/SV9-3990 with UAB "Progressus group".

Institutional Review Board Statement: Not applicable.

Informed Consent Statement: Not applicable.

Data Availability Statement: The data presented in this study are available from the corresponding author upon request. The main results supporting the conclusions are included within the article.

Conflicts of Interest: The authors declare no conflicts of interest.

References

1. Miller, J.D.; Hutchins, M. The impacts of urbanisation and climate change on urban flooding and urban water quality: A review of the evidence concerning the United Kingdom. *J. Hydrol. Reg. Stud.* **2017**, *12*, 345–362. [CrossRef]
2. Liu, N.; Zhang, F. Urban green spaces and flood disaster management: Toward sustainable urban design. *Front. Public Health* **2025**, *13*, 1583978. [CrossRef]
3. Yang, Y.; Zhu, D.Z.; Loewen, M.R.; Zhang, W.; van Duin, B.; Mahmood, K. Impacts of climate change on urban stormwater runoff quantity and quality in a cold region. *Sci. Total Environ.* **2024**, *954*, 176439. [CrossRef]
4. Fletcher, T.D.; Shuster, W.; Hunt, W.F.; Ashley, R.; Butler, D.; Arthur, S.; Trowsdale, S.; Barraud, S.; Semadeni-Davies, A.; Bertrand-Krajewski, J.-L.; et al. SUDS, LID, BMPs and more—The evolution and application of terminology surrounding urban drainage. *Urban Water J.* **2015**, *12*, 525–542. [CrossRef]
5. Jacobson, C.R. Identification and quantification of the hydrological impacts of imperviousness in urban catchments: A review. *J. Environ. Manag.* **2011**, *92*, 1438–1448. [CrossRef]
6. Santamouris, M. Using cool pavements as a mitigation strategy to fight urban heat island—A review of the actual developments. *Renew. Sustain. Energy Rev.* **2013**, *26*, 224–240. [CrossRef]
7. Ahiablame, L.M.; Engel, B.A.; Chaubey, I. Effectiveness of low impact development practices: Literature review and suggestions for future research. *Water Resour. Manag.* **2012**, *26*, 4253–4273. [CrossRef]
8. Scholz, M.; Grabowiecki, P. Review of permeable pavement systems. *Build. Environ.* **2007**, *42*, 3830–3836. [CrossRef]
9. Yu, F.; Guo, J.; Liu, J.; Cai, H.; Huang, Y. A review of the pore structure of pervious concrete: Analyzing method, characterization parameters and the effect on performance. *Constr. Build. Mater.* **2023**, *365*, 129971. [CrossRef]
10. Cui, B.; Luo, A.; Zhang, X.; Huang, P. Research development and key issues of pervious concrete: A review. *Buildings* **2024**, *14*, 3419. [CrossRef]
11. Sha, F.; Zhang, S.M.; Sun, X.C.; Fan, G.X.; Diao, Y.; Duan, X.F.; Wang, H. Mechanical performance and pore characteristics of pervious concrete. *Case Stud. Constr. Mater.* **2024**, *21*, e03674. [CrossRef]
12. Song, H.; Fan, S.; Wan, K.; Yao, J.; Yin, W.; Lee, Y. Balancing mechanical and permeability properties of pervious concrete through inter-aggregate pore structure optimization. *J. Build. Eng.* **2025**, *106*, 112537. [CrossRef]
13. Bean, E.Z.; Hunt, W.F.; Bidelspach, D.A. Evaluation of four permeable pavement sites in eastern North Carolina for runoff reduction and water quality impacts. *J. Irrig. Drain. Eng.* **2007**, *133*, 583–592. [CrossRef]
14. Adewumi, A.A.; Owolabi, T.O.; Alade, I.O.; Olatunji, S.O. Estimation of physical, mechanical and hydrological properties of permeable concrete using computational intelligence approach. *Appl. Soft Comput.* **2016**, *43*, 342–350. [CrossRef]
15. Taheri, B.M.; Ramezanianpour, A.M.; Sabokpa, S.; Gapele, M. Experimental evaluation of freeze-thaw durability of pervious concrete. *J. Build. Eng.* **2021**, *33*, 101617. [CrossRef]
16. Drake, J.; Bradford, A.; Van Seters, T. Hydrologic Performance of Three Partial-Infiltration Permeable Pavements in a Cold Climate over Low Permeability Soil. *J. Hydrol. Engin.* **2014**, *15*. [CrossRef]

17. Ortiz-Marqués, A.; Caldevilla, P.; Goldmann, E.; Safuta, M.; Fernández-Raga, M.; Górski, M. Porosity and permeability in construction materials as key parameters for their durability and performance: A review. *Buildings* **2025**, *15*, 3422. [CrossRef]
18. Hari, R.; Zhuge, Y.; Madhavan, M.K. Strength enhancements and quantitative paradigms in pervious concrete: A review. *Results Eng.* **2025**, *27*, 106668. [CrossRef]
19. Daukšys, M.; Juočiūnas, S.; Vaičiukynienė, D. Vandeniui laidus betonas. *Žemėtvarka Hidrotech.* **2018**, *1*, 49–52.
20. Huang, B.; Wu, H.; Shu, X.; Burdette, E.G. Laboratory evaluation of permeability and strength of polymer-modified pervious concrete. *Constr. Build. Mater.* **2010**, *24*, 818–823. [CrossRef]
21. Kabir, T.; Al-Bayati, H.K.; Tighe, S. Laboratory mix preparation and investigation of mechanical behaviour of polyurethane-bound porous rubber pavement. *Can. J. Civ. Eng.* **2024**, *51*, 1350–1368. [CrossRef]
22. Zhuang, W.; Ding, T.; Pang, C.; Jiao, X.; Geng, L.; Sun, M. Mechanical Properties and Modification Mechanism of Thermosetting Polyurethane-Modified Asphalt. *Coatings* **2025**, *15*, 912. [CrossRef]
23. Lu, G.; Renken, L.; Li, T.; Wang, D.; Li, H.; Oeser, M. Experimental study on the polyurethane-bound pervious mixtures in the application of permeable pavements. *Constr. Build. Mater.* **2019**, *202*, 838–850. [CrossRef]
24. Xu, L.; Lu, T.; Chen, Z.; Ni, H.; Sun, D.; Tian, Y. A review of polyurethane as an alternative to asphalt binder for more sustainable roads: Performance, environment, and economy. *J. Traffic Transp. Eng.* **2024**, *11*, 1268–1290. [CrossRef]
25. Kinay, F.; Bakis, A. Usability of polyurethane resin binder in road pavement construction. *Appl. Sci.* **2025**, *15*, 10592. [CrossRef]
26. *LST EN 14771:2023*; Bitumen and Bituminous Binders—Determination of the Flexural Creep Stiffness—Bending Beam Rheometer (BBR). Lithuanian Standards Board: Vilnius, Lithuania, 2023.
27. *LST EN 12697-18:2017*; Bituminous Mixtures—Test Methods—Part 18: Binder Drainage. Lithuanian Standards Board: Vilnius, Lithuania, 2017.
28. *LST EN 1097-3:2002*; Tests for Mechanical and Physical Properties of Aggregates—Part 3: Determination of Loose Bulk Density and Voids. Lithuanian Standards Board: Vilnius, Lithuania, 2002.
29. *LST EN 12697-5:2019*; Bituminous Mixtures-Test Methods—Part 5: Determination of the Maximum Density. Lithuanian Standards Board: Vilnius, Lithuania, 2019.
30. *LST EN 1015-11:2020*; Methods of Test for Mortar for Masonry—Part 11: Determination of Flexural and Compressive Strength of Hardened Mortar. Lithuanian Standards Board: Vilnius, Lithuania, 2020.
31. MN TRINKELĖS 14. *Methodological Guideline for Paver Works (Chapter IX)*; Order No. V–72, 21 February 2014; Ministry of Environment of the Republic of Lithuania: Vilnius, Lithuania, 2014.
32. *CEN/TS 12390-9:2016*; Testing Hardened Concrete—Part 9: Freeze-Thaw Resistance with De-Icing Salts (CF/CDF). CEN: Brussels, Belgium, 2016.
33. *LST EN 1015-12:2016*; Methods of Test for Mortar for Masonry—Part 12: Determination of Adhesive Strength of Hardened Rendering and Plastering Mortars on Substrates. Lithuanian Standards Board: Vilnius, Lithuania, 2016.
34. *LST EN 1338:2003*; Concrete Paving Blocks-Requirements and Test Methods. Lithuanian Standards Board: Vilnius, Lithuania, 2003.
35. *LST EN 12697-19:2020*; Bituminous Mixtures-Test Methods—Part 19: Permeability of Specimens. Lithuanian Standards Board: Vilnius, Lithuania, 2020.
36. Sumanasooriya, M.S.; Neithalath, N. Pore structure features of pervious concretes proportioned for desired porosities and their performance prediction. *Cem. Concr. Compos.* **2011**, *33*, 778–787. [CrossRef]
37. Gsshosh, S.; Singh, P. A reliability-based optimisation framework for pervious concrete gradation: Balancing strength and permeability under uncertainty. *Results Eng.* **2026**, *30*, 110467. [CrossRef]
38. Valenza, J.J.; Scherer, G.W. A review of salt scaling: II. Mechanisms. *Cem. Concr. Res.* **2007**, *37*, 1022–1034. [CrossRef]
39. Kabir, T.; Tighe, S. Durability evaluation of polyurethane-bound porous rubber pavement for sustainable urban infrastructure. *Constr. Mater.* **2024**, *4*, 382–400. [CrossRef]
40. Hernández-Crespo, C.; Fernández-Gonzalvo, M.; Martín, M.; Andrés-Doménech, I. Influence of rainfall intensity and pollution build-up levels on water quality and quantity response of permeable pavements. *Sci. Total Environ.* **2019**, *684*, 303–313. [CrossRef]
41. Braswell, A.S.; Winston, R.J.; Hunt, W.F. Hydrologic and water quality performance of permeable pavement with internal water storage over a clay soil in Durham, North Carolina. *J. Environ. Manag.* **2018**, *224*, 277–287. [CrossRef]
42. Kabir, T.; Tighe, S. Construction and performance evaluation of polyurethane-bound porous rubber pavement (PRP) trial section in the cold climate. *Sustainability* **2023**, *15*, 2413. [CrossRef]
43. Hung, A.; Li, L.Y.; Swei, O. Evaluation of permeable highway pavements via an integrated life-cycle model. *J. Clean. Prod.* **2021**, *314*, 128043. [CrossRef]
44. Abousnina, R.; Aljuaydi, F.; Benabed, B.; Almabrok, M.H.; Vimonsatit, V. Influence of porosity on the compressive strength of porous concrete for infrastructure applications: A state-of-the-art review. *Buildings* **2025**, *15*, 2311. [CrossRef]
45. Lian, C.; Zhuge, Y. Optimum mix design of enhanced permeable concrete—An experimental investigation. *Constr. Build. Mater.* **2010**, *24*, 2664–2671. [CrossRef]

46. Vijayalakshmi, R. Recent studies on the properties of pervious concrete: A sustainable solution for pavements and water treatment. *Civ. Environ. Eng. Rep.* **2021**, *31*, 54–84. [CrossRef]
47. Xi, Z.; Lu, X. Design and Performance Enhancement of Permeable Pavement Materials: Material Selection, Composition, Structural Design, and Multifunctional Integration in Sponge City Applications—Part 2. In *Infrastructure Development-Innovations, Challenges and Opportunities*; IntechOpen: London, UK, 2026. [CrossRef]
48. Zhu, Y.; Li, H.; Yang, B.; Zhang, X.; Mahmud, S.; Zhang, X.; Yu, B.; Zhu, Y. Permeable pavement design framework for urban stormwater management considering multiple criteria and uncertainty. *J. Clean. Prod.* **2021**, *293*, 126114. [CrossRef]
49. Liu, Q.; Liu, S.; Hu, G.; Yang, T.; Du, C.; Oeser, M. Infiltration capacity and structural analysis of permeable pavements for sustainable urban: A full-scale case study. *J. Clean. Prod.* **2021**, *288*, 125111. [CrossRef]
50. Sičáková, A.; Kováč, M. Relationships between functional properties of pervious concrete. *Sustainability* **2020**, *12*, 6318. [CrossRef]
51. Kia, A.; Delens, J.M.; Wong, H.S.; Cheeseman, C.R. Structural and hydrological design of permeable concrete pavements. *Case Stud. Constr. Mater.* **2021**, *15*, e00564. [CrossRef]